Enhancements to the assimilation of ATMS at ECMWF: Observation error update and addition of NOAA-20

P. Weston, N. Bormann

October 2018

Abstract

The assimilation of microwave radiances from the Advanced Technology Microwave Sounder (ATMS) has been enhanced. Firstly by accounting for inter-channel error correlations and tuning the error variances for the ATMS onboard Suomi National Polar-orbiting Partnership (Suomi-NPP) satellite and secondly by additionally assimilating ATMS radiances from the recently launched NOAA-20 satellite.

Results from accounting for correlated errors show significant improvements to the first guess fits to independent observations including temperature sensitive observations (e.g. AMSU-A, radiosonde temperature), humidity sensitive observations (e.g. MHS, radiosonde humidity) and wind observations. This indicates the change is improving the accuracy of short range temperature, humidity and wind forecasts throughout the atmosphere. Also, extra-tropical geopotential height, wind and temperature forecasts are improved out to 5 days. These positive results led to this change being recommended for implementation with ECMWF cycle 46r1.

A thorough data quality assessment of the NOAA-20 ATMS instrument has been carried out and results indicate that the data before antenna pattern correction is of very good quality. Indications are that the biases are comparable and the newer instrument has lower noise than the Suomi-NPP ATMS for most channels. In addition, the striping present when looking at maps of first guess departures of Suomi-NPP ATMS observations is significantly reduced for NOAA-20 ATMS. Initial assimilation experiments indicate that assimilating the additional NOAA-20 ATMS observations on top of a system already assimilating Suomi-NPP ATMS observations leads to small incremental benefits to temperature, humidity and geopotential height forecasts, particularly in the stratosphere. These results led to the operational introduction of the assimilation of NOAA-20 ATMS data on 22nd May 2018.

The data after antenna pattern correction initially suffered from some asymmetry across the scan. This was caused by some parameters being inherited from Suomi-NPP ATMS whereas the NOAA-20 ATMS instrument turned out to have slightly different characteristics. Recently the antenna pattern correction has been updated and the data after this update look to be of good quality with smaller and more symmetric scan biases than Suomi-NPP ATMS.

1 Introduction

The Suomi-NPP satellite was launched on 28th October 2011 and carries the Advanced Technology Microwave Sounder (ATMS) instrument amongst others. ATMS is a single instrument which combines temperature and humidity sounding channels similar to those from AMSU-A and MHS. Data from ATMS has been operationally assimilated at ECMWF since 26th September 2012. Full details of the initial implementation can be found in Bormann et al. (2013). Since then the use of the data has been extended to include the assimilation of humidity sounding channels and surface sensitive temperature sounding channels over land (Lawrence and Bormann, 2014) and sea ice (Weston et al., 2017).

During the initial implementation, it was found by Bormann et al. (2013) that the ATMS temperature sounding channels had stronger correlated instrument noise than the corresponding AMSU-A channels, and exhibited cross-track striping. This is caused by a low-noise amplifier present on ATMS but not AMSU-A which introduces a 1/f term to the instrument noise (Kim et al., 2014). The period of the 1/f noise term is comparable to the time taken for the instrument to complete one scan line which leads to striping effects to be visible in first guess departure maps of ATMS data. Initially when ATMS was assimilated the assigned observation errors were inflated to indirectly account for these effects.

In recent years a number of NWP centres have started taking account of inter-channel observation error correlations for hyperspectral IR data in their assimilation systems (Weston et al., 2014; Bormann et al.,

2016). These correlations are thought to primarily originate from representation errors rather than characteristics of the instrument noise. In addition, NRL have recently begun taking account of correlated error in the assimilation of ATMS data (Campbell et al., 2017). In this report the impact of directly accounting for inter-channel error correlations for ATMS within the ECMWF assimilation system is assessed.

The first satellite in the Joint Polar Satellite System (JPSS) programme was launched on 18th November 2017 and was named NOAA-20 following the launch. The satellite orbits half an orbit (50 minutes) ahead of Suomi-NPP in the same orbital plane at an altitude of 825km. NOAA-20 carries the same instruments as Suomi-NPP, and in this report the data quality and assimilation impact of the ATMS instrument is assessed. Suomi-NPP and NOAA-20 form part of the Joint Polar System with other NOAA and EUMETSAT satellites and experiences gained with ATMS will be relevant for future instruments such as the MWS on the EUMETSAT MetOp-SG satellites.

The report is organised as follows: the results of the introduction of correlated observation errors for Suomi-NPP ATMS are discussed in section 2; the data quality assessment and initial assimilation experiments of NOAA-20 ATMS are presented in section 3; and future planned work is summarised in section 4.

2 Accounting for inter-channel error correlations in the assimilation of Suomi-NPP ATMS radiances

Figure 1 shows that the assigned observation errors for the ATMS tropospheric and lower stratospheric temperature sounding channels 6 to 11 are significantly larger than the standard deviation of first guess departures for these channels. In contrast, the assigned observation errors for the corresponding MetOp-B AMSU-A channels are a lot closer to the standard deviation of first guess departures. This is the result of recent work to tune the AMSU-A observation errors which has led to significant improvements to forecast accuracy (Bormann et al., 2011; Lawrence et al., 2015).
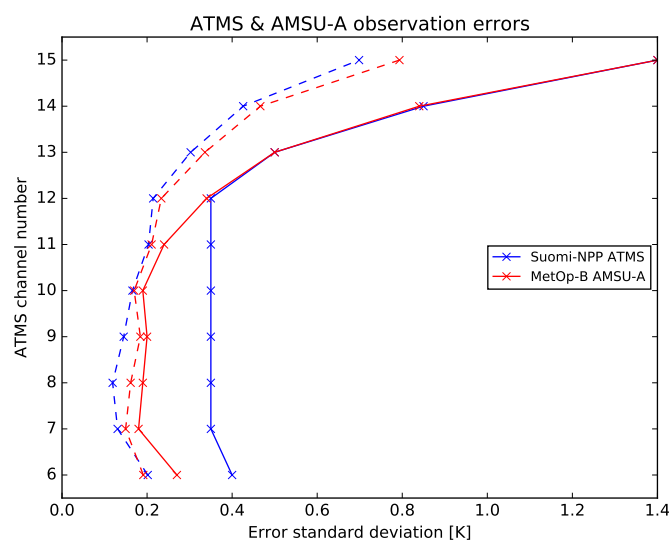
Figure 1: Assigned error standard deviations (solid lines) and standard deviation of first guess departures (dashed lines) for Suomi-NPP ATMS and MetOp-B AMSU-A

The reason the same error tuning has not yet been applied to ATMS is due to the larger inter-channel error correlations between these channels as found by Bormann et al. (2013) (and others) which is largely caused by the 1/f term in the instrument noise introduced by the low-noise amplifier present on ATMS. Campbell et al. (2017) found that accounting for correlated errors when assimilating ATMS allowed the assigned error standard deviations to be closer to the standard deviation of first guess departures and resulted in significant improvements to forecast accuracy.

2.1 Diagnosis of error statistics

2.1.1 Methods

There are several a posteriori methods for estimating error statistics which have become popular in recent years, two of which will be introduced here.

The method proposed by Hollingsworth and Lönnberg (1986) uses the expectation of the product of first guess departures:

$$\mathbf{R} + \mathbf{HBH}^{\mathrm{T}} = E\left[\left(\mathbf{y} - H\left(\mathbf{x}^{\mathrm{b}}\right)\right)\left(\mathbf{y} - H\left(\mathbf{x}^{\mathrm{b}}\right)\right)^{\mathrm{T}}\right] \tag{1}$$

where $\mathbf{R}$ is the observation error covariance matrix, $\mathbf{HBH}^{\mathrm{T}}$ is the background error covariance matrix in observation space, $\mathbf{y}$ are the observations, $\mathbf{x}^{\mathrm{b}}$ is the model background and H is the observation operator.

The innovation covariances calculated in (1) are binned by separation distance. Then the diagnosed observation error statistics are separated from the background error statistics by assuming that background errors are spatially correlated and observation errors are spatially uncorrelated. The relationship between the innovation covariance and separation distance is extrapolated to zero separation to partition the innovation covariances into a spatially correlated part (background error) and a spatially uncorrelated part (observation error).

The method proposed by Desroziers et al. (2005) uses background and analysis departures:

$$\mathbf{R} = E\left[\left(\mathbf{y} - H\left(\mathbf{x}^{\mathrm{a}}\right)\right)\left(\mathbf{y} - H\left(\mathbf{x}^{\mathrm{b}}\right)\right)^{\mathrm{T}}\right] \tag{2}$$

where $\mathbf{x}^{\mathrm{a}}$ is the model analysis. A key assumption in this method is that the assumed $\mathbf{HBH}^{\mathrm{T}}(\mathbf{R} + \mathbf{HBH}^{\mathrm{T}})^{-1}$ is consistent with true error statistics.

Both methods can be used to estimate inter-channel error correlations by sampling first guess and analysis departures from different channels. The Desroziers method can also be used to diagnose spatial and temporal correlations but in this report only inter-channel error correlations are estimated.

For ATMS the assigned observation error is inflated (figure 1) and therefore $\mathbf{HBH}^{\mathrm{T}}(\mathbf{R} + \mathbf{HBH}^{\mathrm{T}})^{-1}$ is unlikely to be consistent with the true error statistics which violates the assumption in the Desroziers method. To reduce the impact of this a combination of the above two methods to diagnose the error statistics as used by Bormann et al. (2016) is used as follows:

1. ATMS first guess departures are used as inputs into the Hollingsworth-Lönnberg method

2. The estimated error standard deviations are inflated by a factor of 1.5, the diagnosed error correlations are not altered and the error covariance matrix is reformed

3. This matrix is then used as the assigned ATMS observation error covariance matrix in an assimilation experiment

4. The first guess and analysis departures from this experiment are then used as inputs to the Desroziers method

5. Finally the estimated error standard deviations are inflated by a range of factors (see section 2.2 for details)

The Hollingsworth-Lönnberg method doesn't make any assumptions about the errors assumed in the assimilation system and only uses first guess departures. Then, this slightly more accurate estimate of the observation error statistics is used in the assimilation system. Finally, the Desroziers method is used on output from this experiment to estimate the final observation error statistics. This should reduce the effect of the violated assumption on the final estimate.

2.1.2   Results

All diagnostic results are calculated from a sample of a month of globally distributed ATMS data. For pragmatic reasons only observation locations where all 15 sounding channels are assimilated are included in the sample. This means observations poleward of 60 degrees latitude, over sea ice or snow, over high orography and where cloud is detected are not used to calculate the statistics. The observations that are included in the calculations come from over ocean and low land areas and should still give a reasonable sample of error structures especially when considering a month of data.
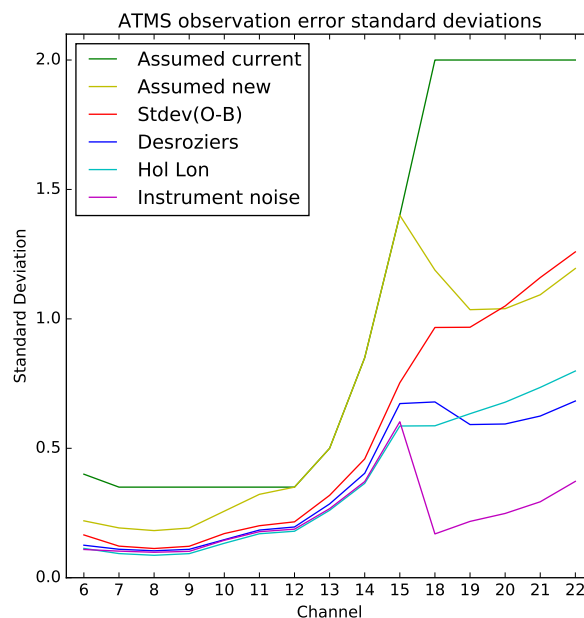
Figure 2: Diagnosed observation error standard deviations compared with assigned error standard deviations and standard deviation of first guess departures for Suomi-NPP ATMS

Figure 2 shows the diagnosed error standard deviations from both the Hollingsworth-Lönnberg and Desroziers methods are significantly smaller than the currently assumed observation errors which is to

be expected as these have been inflated to indirectly account for known inter-channel error correlations. The diagnosed values are also smaller than the standard deviation of first guess departures, especially for the humidity sounding channels. This shows that background errors are larger in humidity than they are in temperature.

The diagnosed values for the temperature sounding channels are very close to the instrument noise showing that the instrument noise dominates the observation error for these channels and other sources of error are negligible. For the humidity sounding channels the instrument noise is significantly smaller than the diagnosed errors suggesting that other sources of error such as representation, forward model and pre-processing errors are larger for these channels.

The instrument noise should provide a lower bound for the diagnosed values, however for some of the channels the Hollingsworth-Lönnberg method yields smaller diagnosed errors than the instrument noise. This may be caused by non-zero horizontal observation error correlations which are assumed to be zero in this method. These correlations could be caused by pre-processing errors such as undetected cloud or uncertainties in surface emissivity and previous studies have suggested that horizontal error correlations are non-zero for some observations (Bormann and Bauer, 2010).

Comparing the diagnosed values from the Desroziers and Hollingsworth-Lönnberg methods shows that the Desroziers estimates are generally larger for the temperature sounding channels but they agree reasonably well which gives confidence that the estimates are reliable. However, there are some noticeable differences in the humidity sounding channels where the Desroziers method gives a larger value for the lowest peaking channel 18 but smaller values than the Hollingsworth-Lönnberg method for the other four channels. This may be because the background errors are larger (and more comparable in magnitude to the observation errors) for these channels which may result in more inaccuracies in the estimates when trying to split the observation and background errors from the innovations.

Figure 3 shows that the most strongly correlated channels are neighbouring humidity sounding channels. The next most significant block of correlations is between the four tropospheric temperature sounding channels. The final block of channels are the stratospheric temperature sounding channels which have significantly weaker inter-channel error correlations than the other channels.

Comparing the diagnosed matrices in figure 3 (a) and (b) to the instrument noise correlation matrix in (c) gives some idea of the sources of the various blocks of correlations. The instrument noise correlation matrix was measured during the pre-launch thermal vacuum tests of the instrument and is independent of NWP fields. The source of the instrument noise correlations is the 1/f term from the low noise amplifier which is correlated between channels (Kim et al., 2014). Qualitatively the structures of the instrument noise and diagnosed correlation matrices do look quite similar showing that the 1/f term is a significant contribution to the overall inter-channel correlations. This was also the conclusion of Bormann et al. (2013) who showed that the diagnosed correlations between the ATMS temperature sounding channels, with the low noise amplifier, are significantly larger than those for the corresponding AMSU-A temperature sounding channels, without the low noise amplifier.

For the stratospheric temperature sounding channels 10 to 15 the structures of the correlations in the instrument noise and diagnosed matrices are very similar with the magnitude of the instrument noise correlations only slightly weaker than the diagnosed correlations. There is also a significant contribution from the correlated instrument noise to the diagnosed correlations between the four tropospheric temperature sounding channels 6 to 9. However, the instrument noise correlations are weaker than the diagnosed correlations suggesting there is another significant source. These channels are sensitive to cloud and, although the sample used to calculate the statistics should be cloud-free, there may be some imperfections in the cloud detection algorithms leading to undetected cloud affecting the statistics for

(a)

(b)

(c)
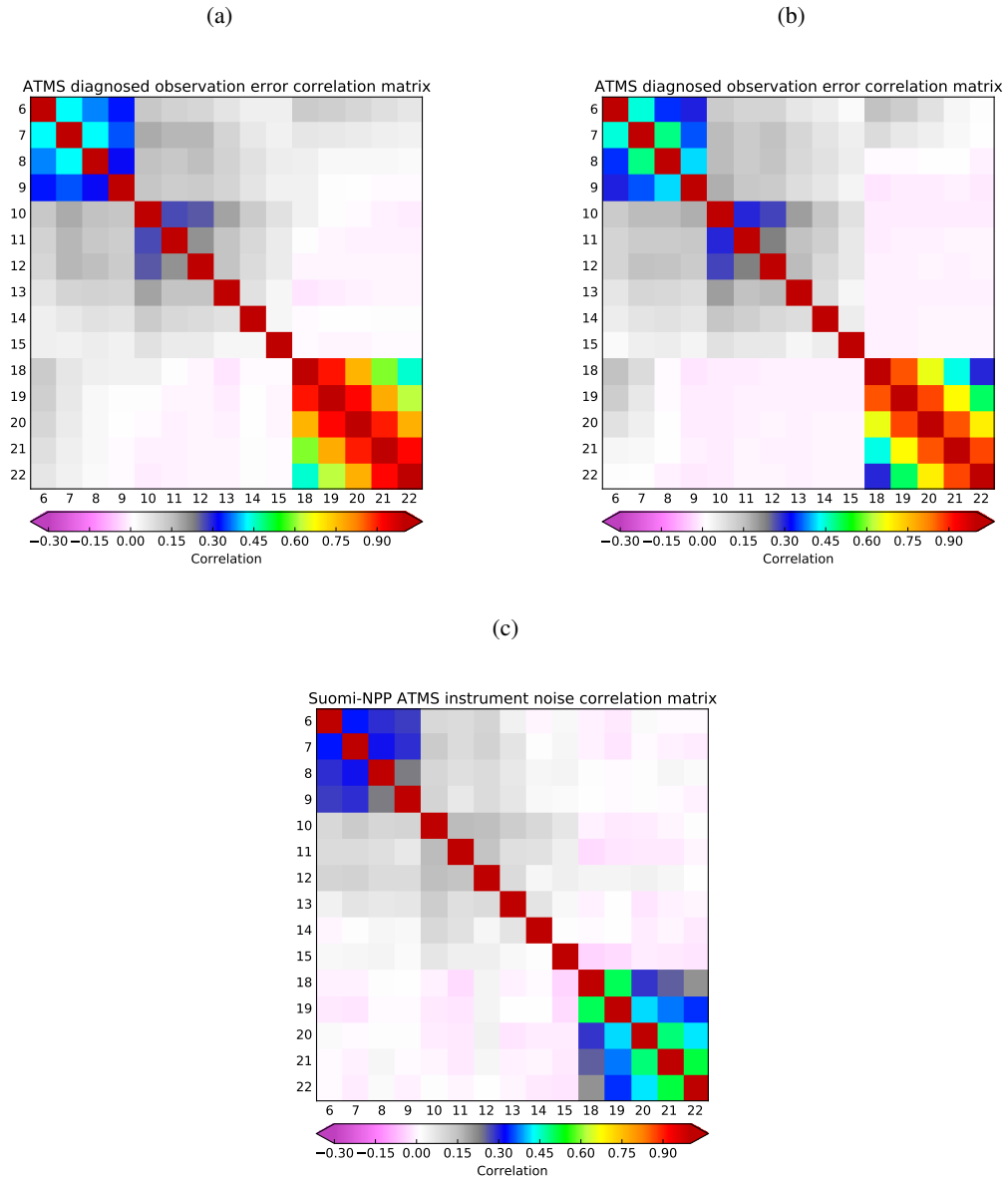
Figure 3: Diagnosed observation error correlation matrices for Suomi-NPP ATMS using: (a) the Hollingsworth-Lönnberg method; (b) the Desroziers method; (c) the instrument noise correlation matrix

these channels. Given the sample used only actively assimilated data these are important features to represent. There may also be a contribution from inaccurate skin temperature or surface emissivity in the lowest peaking channels especially over land where these parameters have larger uncertainties than over ocean. These aspects may motivate the use of different error covariance matrices over land and ocean but an investigation into this is left to a future study.

The strongest block of correlations is between the humidity sounding channels 18 to 22 in both the diagnosed and instrument noise matrices. However, there is a large difference in the magnitude of these correlations which suggests that the instrument noise is not the dominant source of these correlations. The most likely source of these correlations is from errors of representation where the relatively small-scale humidity features in the observations are mismatched with the larger scale humidity features represented in the model. This is consistent with results seen for other microwave and infrared humidity sounding channels (Bormann and Bauer, 2010; Weston et al., 2014).

Figure 3 also shows that the diagnosed inter-channel error correlations are largely similar from the two methods which again gives some confidence in the reliability and accuracy of the estimates. The most noticeable differences are the slightly stronger correlations between channels 6 to 9 given by the Desroziers method and the sharper drop off in correlations between non-neighbouring humidity sounding channels 18 to 22 from the Desroziers method.

2.2 Experiments

Seasons	Cycle	Description
		Initial experiments
Summer 2016 & Winter 2016/17	43r3	Control
Summer 2016 & Winter 2016/17	43r3	ATMS correlated errors with x1.0 inflation
Summer 2016 & Winter 2016/17	43r3	ATMS correlated errors with x1.25 inflation
Summer 2016 & Winter 2016/17	43r3	ATMS correlated errors with x1.5 inflation
Summer 2016 & Winter 2016/17	43r3	ATMS correlated errors with x1.75 inflation
Summer 2016 & Winter 2016/17	43r3	ATMS correlated errors with x2.0 inflation
		Final experiments
Summer 2017 & Winter 2016/17	45r1	Control
Summer 2017 & Winter 2016/17	45r1	ATMS correlated errors with x1.75 inflation (and channels 12-15 with original inflated errors)

Table 1: Summary of experiments to test the ATMS correlated error changes

Initial experiments were run over two periods of four months each: 1st June 2016 to 30th September 2016 and 1st November 2016 to 28th February 2017. The experiments used the configuration of cycle 43r3 of the IFS and ran at $T_{CO}399$ (28km) forecast resolution with the first, second and third inner loops

of the assimilation minimisation run at T_L95 (170km), T_L159 (120km) and T_L255 (80km) resolutions respectively.

The aim of the initial experiments is to ascertain what level of inflation of the diagnosed error standard deviations gives optimal results. These experiments are motivated by previous attempts to account for error correlations where some form of inflation has been necessary to optimise results (Weston et al., 2014; Bormann et al., 2016).

Final experiments were run over two periods of three months each: 1st December 2016 to 28th February 2017 and 1st June 2017 to 31st August 2017. The experiments used the configuration of cycle 45r1 of the IFS and ran at the same resolution as the initial experiments. Table 1 shows the exact configurations run for both the initial and final experiments. The error standard deviations used in the final experiments are shown as the yellow line in figure 2.

Variational quality control (VarQC) is used to down-weight or reject observations which are anomalous compared to other neighbouring observations (Anderson and Järvinen, 1999). Currently it is prohibitively expensive to run VarQC for observations where correlated errors are directly accounted for. One option which is currently being experimented with for all sky data is to apply VarQC to departures pre-multiplied by the matrix of eigenvectors of the correlated **R** matrix (Alan Geer, personal communication). However, this is not currently an option for ATMS due to the situation dependent selection of channels over different surfaces and when cloud is detected.

Therefore in all of the experiments which account for ATMS correlated errors, VarQC is switched off for ATMS. To measure the impact of switching off VarQC for ATMS an additional experiment was run to test this in isolation. The impact was largely neutral with some small degradations to first guess fits to humidity sensitive observations. These degradations were more than compensated by the improvements coming from accounting for correlated errors.

2.3 Results
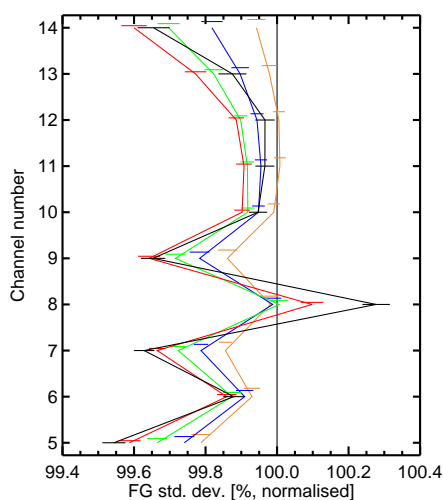
Figure 4: Change in global standard deviation of first guess departures for AMSU-A when ATMS correlated errors are used with error standard deviations inflated by 1.0 (black), 1.25 (red), 1.5 (green), 1.75 (blue), 2.0 (cyan) against the control experiment

Figure 4 shows that the largest improvements to the first guess fits for the lower to mid tropospheric peaking AMSU-A channels 5 to 7 are attained with no inflation applied to the error standard deviations. However, using the error standard deviations with no inflation also result in a degraded fit to AMSU-A channel 8 sensitive around the tropopause and this choice is not optimal when considering the change in first guess fits to the stratospheric channels 9 to 14. The degradation to AMSU-A channel 8 is still present when using the 1.25 inflation so a better compromise would be to use either a 1.5 or 1.75 inflation factor as the results with these choices still maintain the majority of the improved fits to AMSU-A channels 5 to 7, 9 to 14 as well as a neutral impact on channel 8. The reasons for the apparently anomalous behaviour of AMSU-A channel 8 will be investigated later in this section. The first guess fits for other observation types showed similar results with the largest improvements when using the error standard deviations with inflation factors of 1.25 or 1.5.
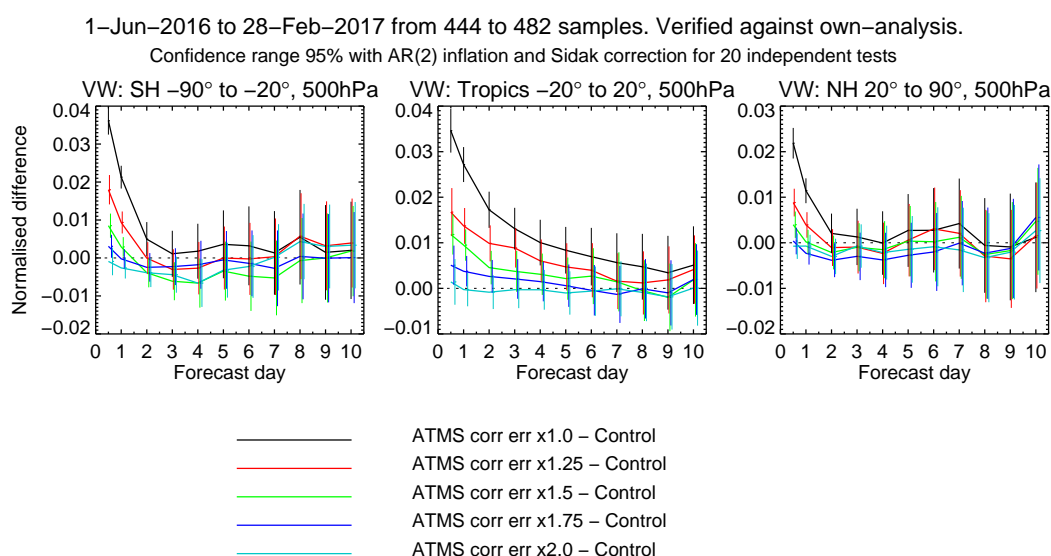
Figure 5: Change in RMSE of vector wind forecasts when ATMS correlated errors are used with error standard deviations inflated by 1.0 (black), 1.25 (red), 1.5 (green), 1.75 (blue), 2.0 (orange) against the control experiment for the Southern extra-tropics (left), tropics (centre) and Northern extra-tropics (right)

Figure 5 shows that there are significant degradations to vector wind forecasts globally at short range but also extending into the medium range in the tropics when using the smaller inflation factors of 1.0, 1.25 and even 1.5. These degradations are also apparent in temperature and geopotential height forecasts (not shown). For the larger inflation factors such as 1.75 and 2.0 the forecast scores become more neutral in the tropics and there are some improvements in the extra-tropics.

Weighing up the results from both the first guess fits and the forecast scores it was decided that the final configuration should use error standard deviations inflated by 1.75 as a compromise between the better forecast scores at larger inflation factors and the better first guess fit improvements at smaller inflation factors. Coincidentally this is the same inflation factor that Bormann et al. (2016) found to produce optimal results when specifying correlated observation errors for IASI.

There are several possible reasons for the need to inflate the error standard deviations to obtain optimal results. It may be due to inaccurate initial estimates from the a posteriori methods due to the violated assumptions in their calculation. Or it could be due to sub-optimalities in the specification of the background error. It could also be due to neglected horizontal error correlations. Finally, the diagnosed

observation errors are global averages so there may be areas or situations where the true observation errors are significantly smaller than the diagnosed ones and vice versa. In variational data assimilation if an assumed observation error is smaller than the true observation error then the analysis produced may be less accurate than the background (Eyre and Hilton, 2013). By inflating the assumed observation errors, degradations are avoided in areas where the diagnosed errors are smaller than the true errors, whereas improvements are reduced in areas where the diagnosed errors are equal to or larger than the true errors. Moving to a more situation dependent observation error model (as is done in all-sky assimilation at ECMWF e.g. Geer et al. (2014)) may reduce the need to inflate the diagnosed observation error estimates to optimise results when used in the assimilation system. These aspects are subjects of active research.

In the initial experiments the observation errors for all channels used the newly diagnosed (and inflated) error standard deviations. Previous attempts to tune the errors in the AMSU-A stratospheric channels 11 to 14 (equivalent to ATMS channels 12 to 15) led to instabilities in the assimilation system and some forecast degradations. For this reason the observation errors for only AMSU-A channels 6 to 10 were reduced by Bormann et al. (2011). In the ATMS experiments there were some forecast degradations at longer ranges in the stratosphere for vector wind, temperature and geopotential height (not shown). These degradations led to the decision to keep the observation error standard deviations at their previous values for the stratospheric ATMS channels 12 to 15 in the final configuration.
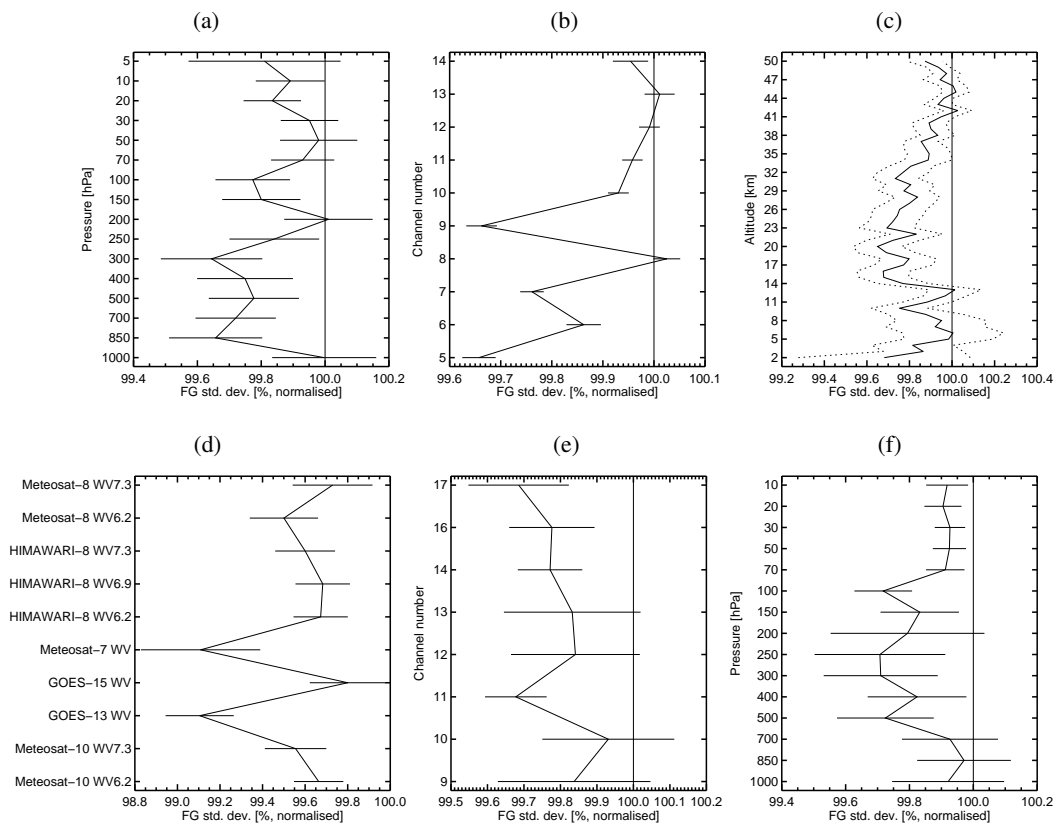
Figure 6: Change in global standard deviation of first guess departures for (a) radiosonde temperature, (b) AMSU-A, (c) GPSRO, (d) Geostationary clear sky radiances, (e) SSMIS, and (f) conventional wind observations for the final ATMS correlated observation error configuration against the control experiment

Figure 6 shows that the final configuration of the correlated ATMS observation errors results in significantly improved first guess fits to a range of observation types. Panels (a), (b) and (c) show improved fits to radiosonde temperature, AMSU-A channels 5 to 7 and 9 to 11 and GPSRO bending angles in the stratosphere. This indicates that short-range temperature forecasts throughout the atmosphere are improved. Panels (d) and (e) show improved fits to infrared clear sky radiances on geostationary satellites and all sky microwave radiances from SSMIS. This indicates that short-range tropospheric humidity forecasts are improved. Finally, panel (f) shows improved fits to conventional wind forecasts particularly above 700hPa indicating improved short-range wind forecasts.

As seen in figure 6 the first guess fits to most observations are improved by this change. Figure 7 shows that the first guess fits to most CrIS channels are also improved, particularly the tropospheric temperature sounding channels between 698cm^{-1} and 810cm^{-1} and also the humidity sounding channels around 1562cm^{-1}. However, there is a small group of channels with frequencies around 695cm^{-1} where there are degraded fits. The peak sensitivity of these channels is around the tropopause and there are also slightly weaker degraded fits to the corresponding IASI channels. This would also appear to be linked to the anomalous neutral first guess fit (and degradations when using smaller inflation factors) of AMSU-A channel 8 which is also sensitive to the temperature around the tropopause. It is worth noting that in the initial experiments with smaller inflation factors the degradations to these CrIS channels were significantly stronger (not shown).
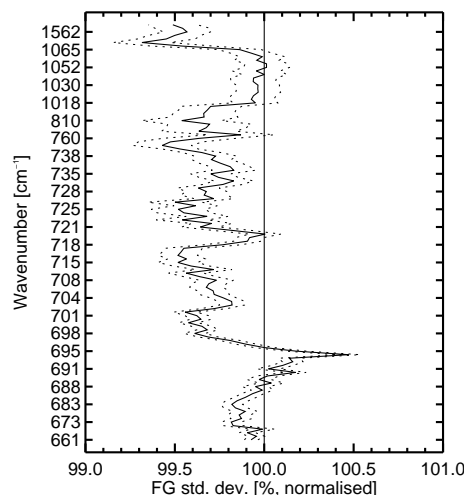
Figure 7: Change in global standard deviation of first guess departures for CrIS when ATMS correlated errors are used with error standard deviations inflated by 1.75 against the control experiment

To further investigate the origin of these degradations we examine the eigenstructure of the new error covariance matrix. Figure 8 shows that the leading eigenvector has large contributions from all of the humidity sounding channels while the trailing eigenvector has contributions of opposite signs in the upper tropospheric temperature sounding channels. Bormann et al. (2016) showed that observations with first guess departures which map on to the leading eigenvectors of the observation error covariance matrix will be given relatively less weight than observations with first guess departures which map on to the trailing eigenvectors. This means that observations which have first guess departures with broad vertical scales in humidity will be down-weighted compared to the control. This could be beneficial, particularly as departures with this structure may indicate unwanted cloud contamination in the observation. However, observations which have first guess departures with sharp vertical scales, such as around the tropopause, will be up-weighted compared to the control. Therefore the hypothesis is that the observations of the

sharper vertical scales and features are potentially being over-fitted resulting in the degraded fits to the infrared channels sensitive around the tropopause where the vertical structure of the atmosphere is important. One possible solution to this is to inflate only the smallest eigenvalues and then reform the matrix as has been done at both the Met Office and ECMWF for IASI (Weston et al., 2014; Bormann et al., 2016). Initial experimentation suggests that this may indeed be beneficial and this will be the subject of future work.
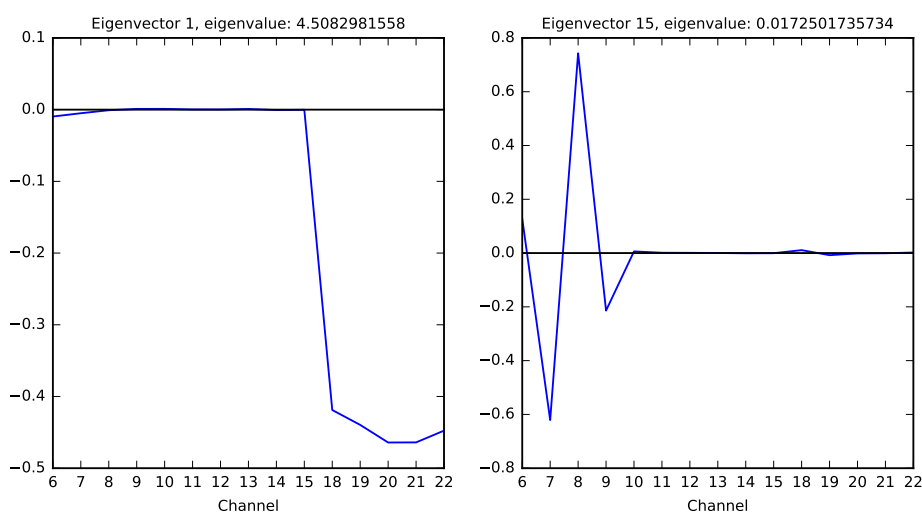
Figure 8: Leading and trailing eigenvectors of the observation error covariance matrix used in the final assimilation experiments

Using the final configuration of the ATMS correlated errors results in significantly improved forecasts of vector wind and geopotential height in the extra-tropics (figure 9). The magnitude of these improvements are 0.5-1% which are statistically significant out to T+72 in the Southern hemisphere. These improvements are comparable to the impact obtained when introducing the assimilation of a completely new microwave instrument into the system (Geer, 2016). When verified against operational analyses there are also similar improvements to the temperature and relative humidity forecasts in the extra-tropics. Radiosonde based forecast verification also shows significant improvements to forecast accuracy for the same variables and regions.

When verifying against own analyses there are mean changes to the analysis which result in apparent degradations to temperature and relative humidity at short forecast ranges. For example, figure 10 shows a significant warming of up to 0.2K and moistening of up to 1.5% in relative humidity in the analysis at 850hPa over the Southern Ocean. This leads to larger RMSE of temperature (figure 11) and relative humidity forecasts out to T+48 in this area when verified against own analyses. However, observation based verification indicates that these mean changes are correcting an existing model cold and dry bias. In addition, when verifying against operational analyses the short-range forecasts of relative humidity and temperature in this area are improved. Also, figure 11 shows that forecasts from T+72 to T+216 show a significant and consistent improvement in temperature in this area when verified against own analyses and this improvement is also present for relative humidity (not shown).
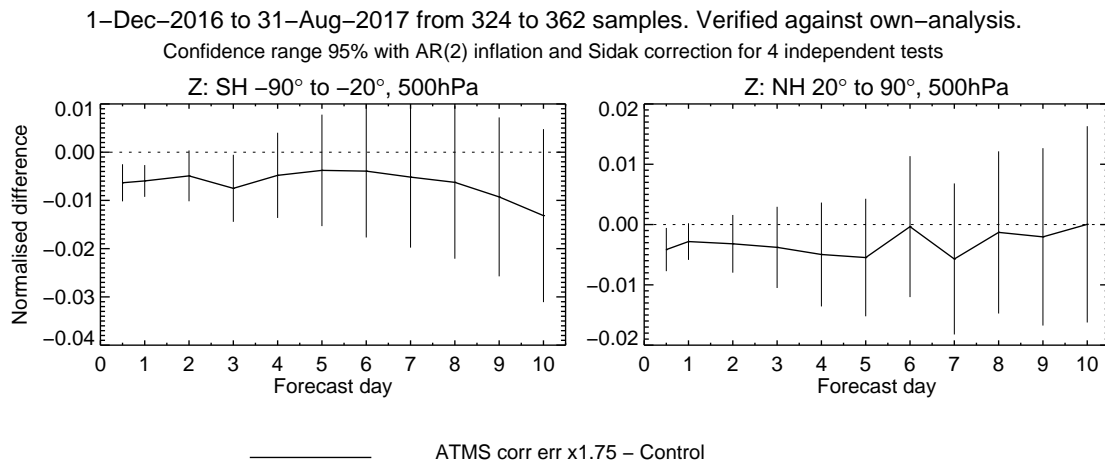
Figure 9: Change in RMSE of 500hPa geopotential height forecasts verified against own analyses when the final configuration of ATMS correlated errors are used against the control experiment for the Southern extra-tropics (left) and Northern extra-tropics (right)

The forecast scores in the tropics are mostly neutral with some apparent degradations caused by changes to the mean analysis. For example, figure 10 shows a mean cooling and moistening of the analysis at 850hPa in the stratocumulus areas off the West coasts of South America and Africa. This is causing apparent forecast degradations in temperature (figure 11) and humidity (not shown) when verifying against own analyses. Lonitz and Geer (2017) illustrated a model bias in these areas which appears in mean normalised first guess departure maps of microwave imager observations, e.g. their figure 2b. There are positive departures in the stratocumulus regions which indicates that the model is too warm and dry compared to the observations. They also showed that assimilating microwave imager observations, which have the same cooling and moistening effect on the mean analysis as the ATMS correlated errors change, in these areas were beneficial when verifying forecasts against other independent observations. Therefore, given the ATMS correlated errors are making similar changes to the analysis it is believed this change is improving the quality of the analysis in these regions.

An additional experiment was run where a diagonal assumed observation error covariance matrix was used. This matrix consisted of the inflated Desroziers diagnosed error variances with the correlations set to zero. This experiment was then compared to those using the full error covariance matrix to ascertain whether most of the impact is coming from the smaller diagonal error variances or including the correlations. The results showed that most of the impact in temperature is coming from the smaller variances but with a small additional improvement when the correlations are introduced. For humidity the impact is dominated by the introduction of the correlations with the smaller variances being a less important change. This is to be expected given the strongest correlations are between the humidity sounding channels.

2.4 Summary

Accounting for correlated observation errors in the assimilation of ATMS leads to significantly improved first guess fits to the vast majority of observations as well as small but significant improvements to the extra-tropical forecast scores. There are also some significant mean changes to the analysis as a result of the ATMS correlated errors which generally seem to improve fits to other observations despite causing apparent degradations to forecasts when verifying against own analyses. When verified against

(a)

(b)
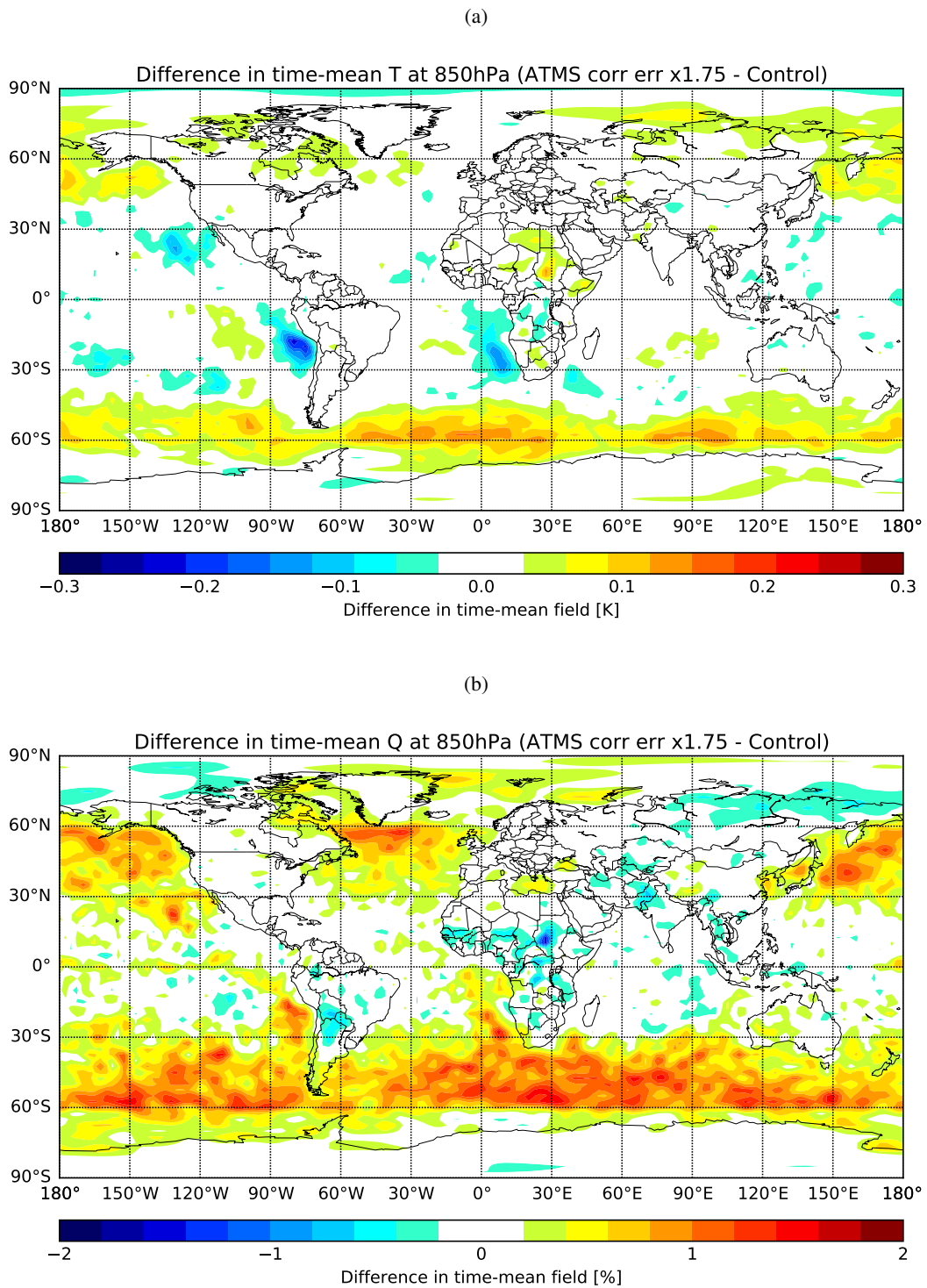
Figure 10: Mean change to the analysis in (a) 850hPa temperature, (b) 850hPa relative humidity for the final ATMS correlated observation error configuration against the control experiment

Change in error in T (ATMS corr err x1.75 – Control)

1–Dec–2016 to 31–Aug–2017 from 324 to 362 samples. Verified against own–analysis.
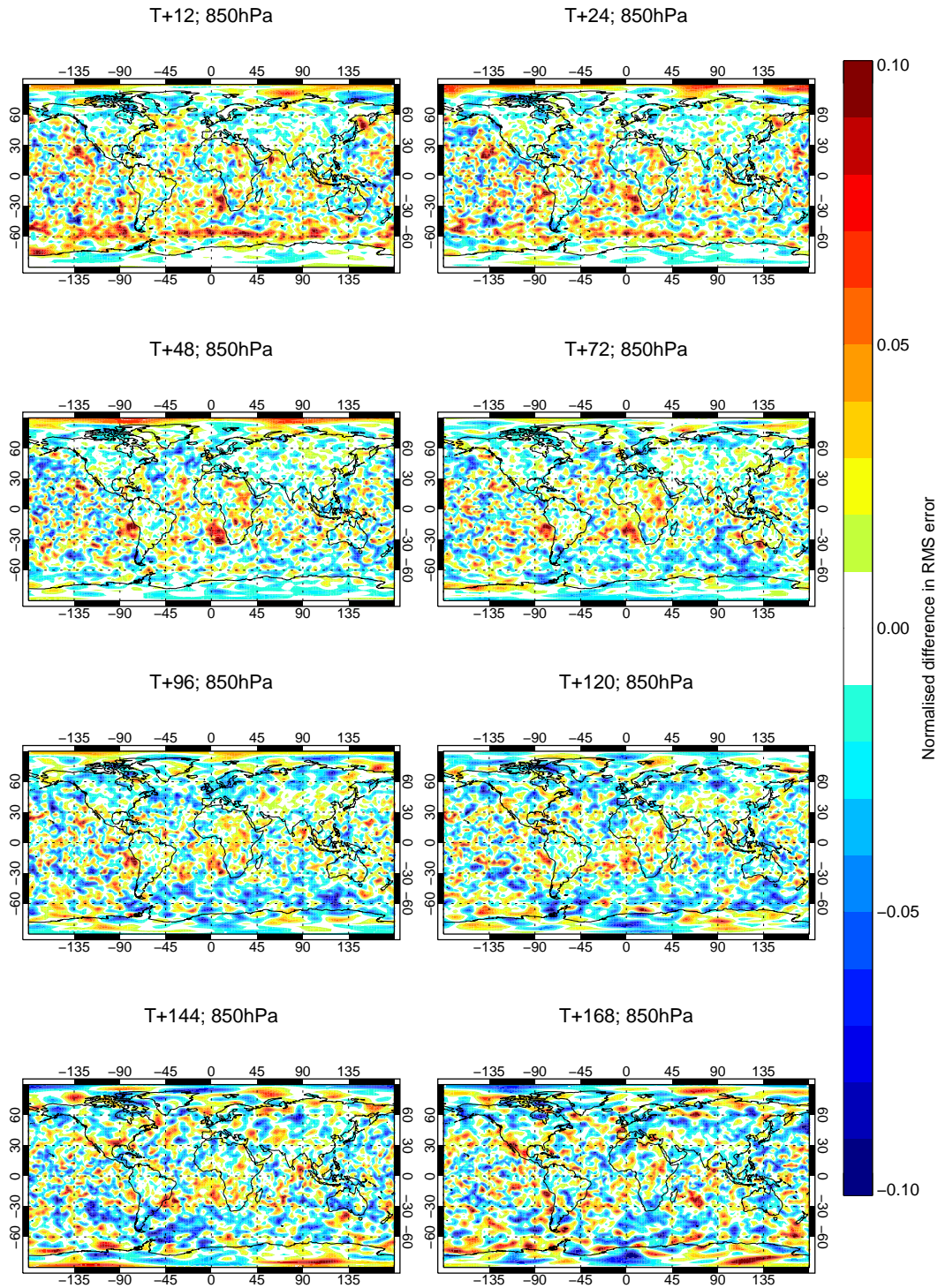
Figure 11: Change in RMSE of 850hPa temperature forecasts verified against own analyses when the final configuration of ATMS correlated errors are used against the control experiment

observations or operational analyses the extra-tropical forecasts are improved by 0.5-1%.

Based on this evidence the implementation of the use of ATMS correlated observation errors was recommended for inclusion with ECMWF cycle 46r1.

3 NOAA-20 ATMS

The NOAA-20 satellite was launched on 18th November 2017 and in this section data from the ATMS instrument onboard NOAA-20 is assessed post launch. A near real-time data feed from NOAA-20 ATMS was set up by EUMETSAT from mid February 2018 which allowed a thorough data quality assessment starting just a few months after launch. Initially the NOAA-20 ATMS data was used in the ECMWF data assimilation system with the same configuration as the Suomi-NPP ATMS is currently used. This included the same pre-processing, 3x3 averaging to give comparable spatial resolution and noise characteristics as AMSU-A, cloud screening, thinning and bias correction predictors. The assumed observation error covariance matrix is diagonal with error standard deviations as currently used for Suomi-NPP. More details of this configuration can be found in Bormann et al. (2013).

3.1 Data quality assessment

The quality of the NOAA-20 ATMS radiances can be assessed by comparing the data to short-range forecasts from the ECMWF Integrated Forecast System (IFS) transformed into radiance space using a clear-sky radiative transfer model. The differences between the observations and their model equivalents are called first guess departures and the statistics of these departures can be analysed and compared to other similar instruments to gauge the quality of the NOAA-20 ATMS data.
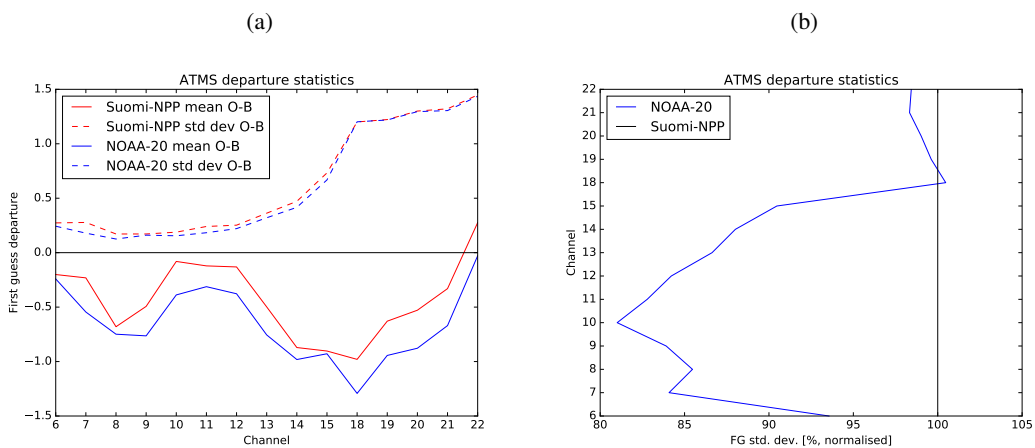
Figure 12: Global first guess departure statistics for NOAA-20 and Suomi-NPP ATMS assimilated channels before antenna pattern correction, after quality control: (a) mean and standard deviation of first guess departures before bias correction and (b) standard deviation of first guess departures normalised by Suomi-NPP ATMS after bias correction. Statistics were accumulated between 22nd and 29th March 2018

Initially the NOAA-20 ATMS data before antenna pattern correction (also known as the technical data

records (TDRs)) are assessed as the initial antenna pattern correction used to convert the TDRs to sensor data records (SDRs) was not accurate. This was because it inherited properties from Suomi-NPP ATMS which has a larger reflector emissivity than NOAA-20 ATMS. There is more discussion and analysis of the data before and after antenna pattern correction later in this section. In the ECMWF assimilation system Suomi-NPP ATMS data is assimilated after antenna pattern correction and so, to be consistent, it would be preferred to also assimilate NOAA-20 ATMS data after antenna pattern correction.

(a)   (b)

(c)   (d)
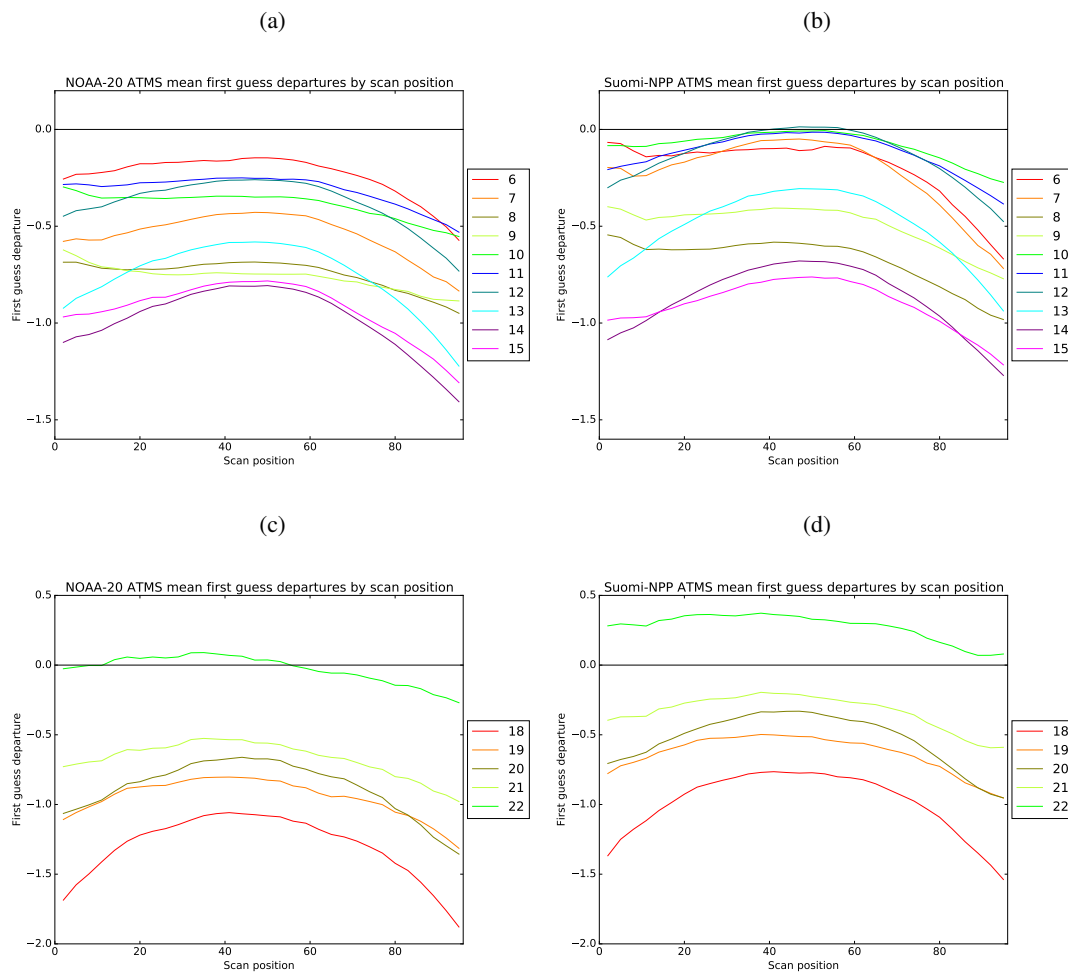
Figure 13: Mean first guess departures before bias correction binned by scan position for NOAA-20 (left) and Suomi-NPP (right) ATMS temperature sounding channels (top) and humidity sounding channels (bottom). Statistics are for data after quality control and were accumulated between 22nd and 29th March 2018

Figure 12 (a) shows that NOAA-20 ATMS has slightly larger biases than Suomi-NPP ATMS. For most channels the differences are fairly constant at around 0.2-0.3K and this quasi-constant offset should be straightforwardly corrected by the variational bias correction scheme (VarBC) run as part of the ECMWF assimilation system. Figure 12 (b) shows that the standard deviation of first guess departures are significantly smaller for most channels for NOAA-20 ATMS than for Suomi-NPP ATMS. The largest differences are in the upper tropospheric and lower stratospheric peaking channels 9 to 12 where the standard deviations of first guess departures for NOAA-20 ATMS are more than 15% smaller than for Suomi-NPP

ATMS and the differences are more than 5% for all temperature sounding channels 6 to 15. The values are more similar for the humidity sounding channels 18 to 22. These differences can be attributed to smaller instrument noise for NOAA-20 ATMS compared to Suomi-NPP ATMS (Nigel Atkinson, personal communication).

Figure 13 shows that the scan position dependent biases are fairly symmetric for both the temperature and humidity sounding channels for NOAA-20 ATMS. They are similar in shape and symmetry to the scan position dependent biases for the corresponding channels on Suomi-NPP ATMS but the biases for NOAA-20 ATMS are slightly more negative by 0.2-0.3K for most channels. This is consistent with what was seen in the global statistics in figure 12. The air mass dependent biases were also assessed and the same results were found that the patterns were similar between NOAA-20 and Suomi-NPP ATMS but that NOAA-20 ATMS biases were slightly more negative.

As previously mentioned in section 2 Suomi-NPP ATMS is affected by correlated instrument noise due to a 1/f contribution coming from a low noise amplifier. This manifested itself in spatially correlated errors visible as stripes in maps of first guess departures. Figure 14 shows a comparison of the striping visible in the Suomi-NPP and NOAA-20 ATMS channel 12 observations. Qualitatively, it appears that the striping is reduced for NOAA-20 but not completely removed.
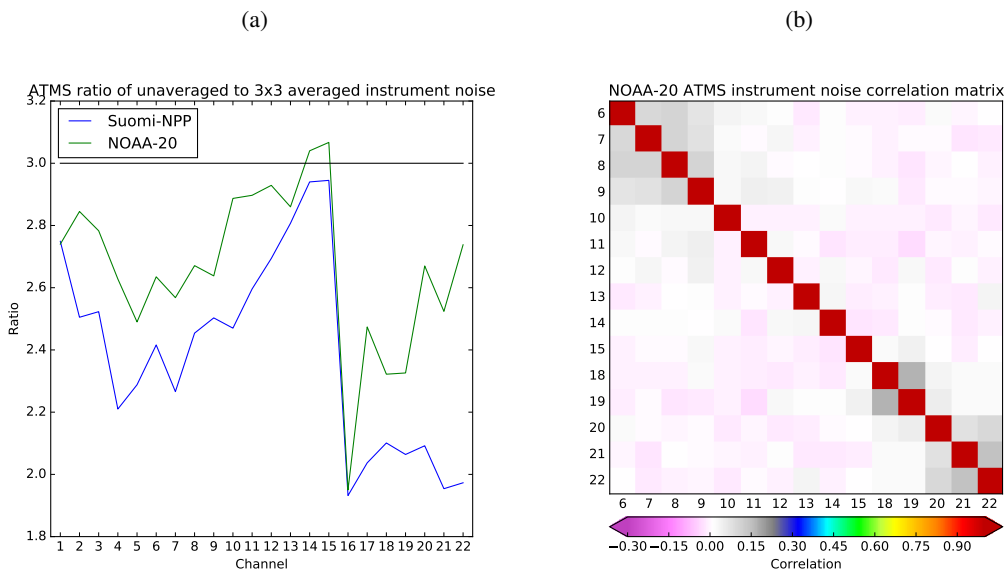
Figure 15: (a) Ratio of noise equivalent delta temperature (NEDT) for unaveraged ATMS warm counts to NEDT for 3x3 averaged ATMS warm counts and (b) NOAA-20 ATMS noise correlation matrix

Figure 15 (a) shows a more quantitative method of measuring the effect of the 1/f noise on the overall noise characteristics of the NOAA-20 and Suomi-NPP data. The ratio between the NEDT of the unaveraged ATMS data and the NEDT of the 3x3 averaged ATMS data should be 3 if the noise is perfectly Gaussian. If the ratio is less than 3 this indicates that there is a contribution from some form of 1/f or non-Gaussian noise. The values of this ratio are closer to 3 for NOAA-20 compared to Suomi-NPP suggesting that the 1/f noise is less dominant for NOAA-20 than Suomi-NPP. However, for some channels the value of this ratio is still significantly smaller than 3 for NOAA-20 showing that there is still a small contribution from the 1/f noise. Figure 15 (b) shows the NOAA-20 ATMS instrument noise correlation matrix which, when compared to figure 3 (c), suggests that the instrument noise is much less correlated

(a)

NOAA-20 ATMS channel 12 first guess departure 2018030500

(b)

Suomi-NPP ATMS channel 12 first guess departure 2018030500
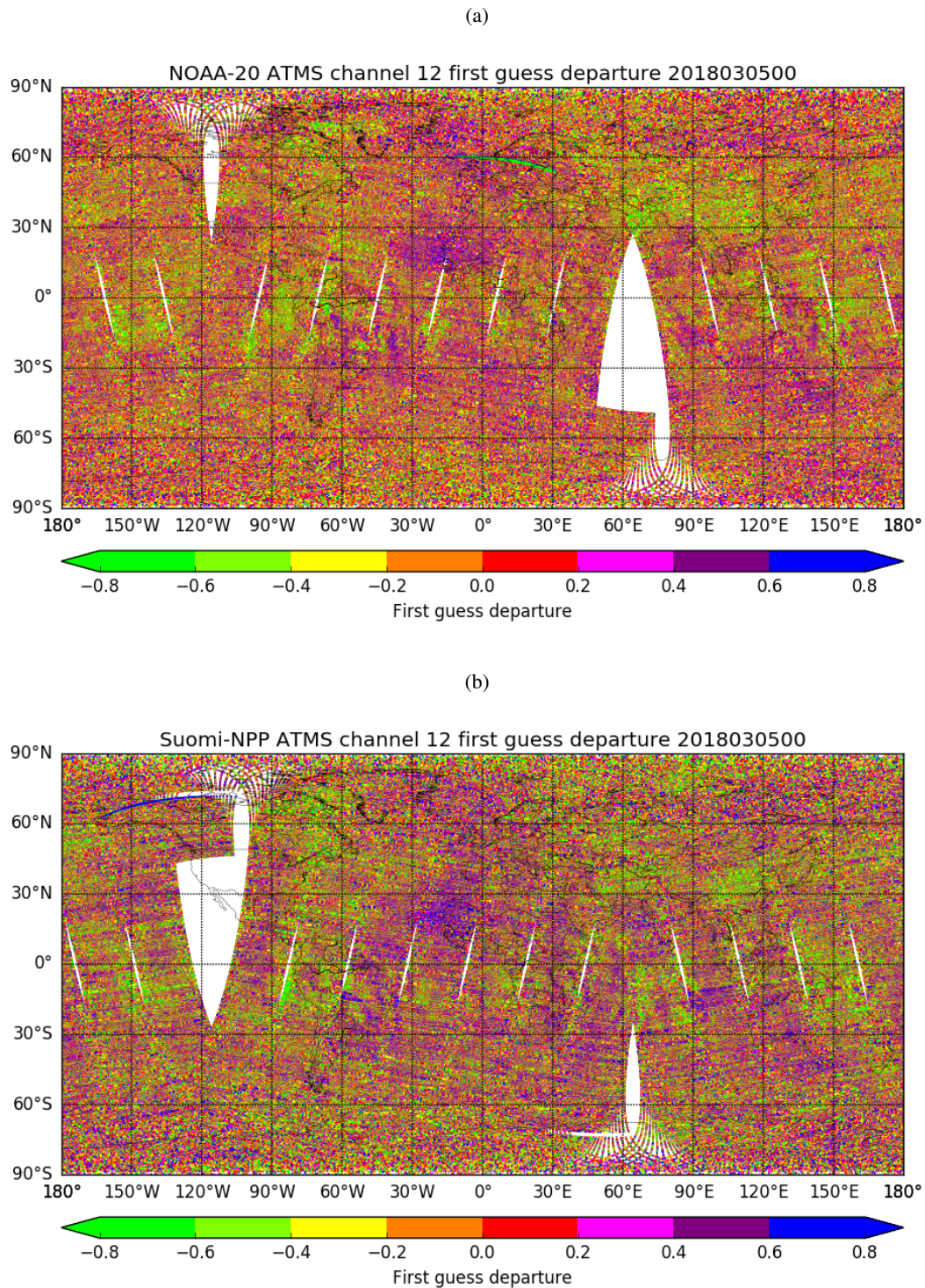
Figure 14: Maps of first guess departures after bias correction for (a) NOAA-20 and (b) Suomi-NPP
ATMS channel 12. The data is unaveraged, before quality control and covers the period between
21UTC on 4th March 2018 and 9UTC on 5th March 2018

between channels for NOAA-20 ATMS than it is for Suomi-NPP. The reasons behind the weaker striping and inter-channel error correlations for NOAA-20 are unclear, but are likely due to hardware difference as the low noise amplifiers on NOAA-20 were manufactured by different companies (Kent Anderson, personal communication) than for Suomi-NPP.

Previously the results shown have all been for the TDRs i.e. before antenna pattern correction. Figure 16 shows results for the SDRs i.e. after antenna pattern correction. Panel (a) shows that the original version of the antenna pattern correction introduced a large asymmetry into the scan position dependent biases. VarBC uses a third order polynomial to correct scan position dependent biases which means it was only partially able to correct these biases due to the shape of this bias curve across the scan. This also led to significantly larger standard deviations of the first guess departures before and after bias correction. Due to these effects the data after antenna pattern correction couldn't be used effectively in our assimilation system so the data before antenna pattern correction was used instead and feedback was given to NOAA. The response from NOAA was that the original NOAA-20 ATMS antenna pattern correction had inherited parameters from the Suomi-NPP ATMS antenna pattern correction but due to a smaller reflector emissivity on NOAA-20 new parameters needed to be calculated for the NOAA-20 antenna pattern correction (Hu Yang, personal communication).

(a)   (b)
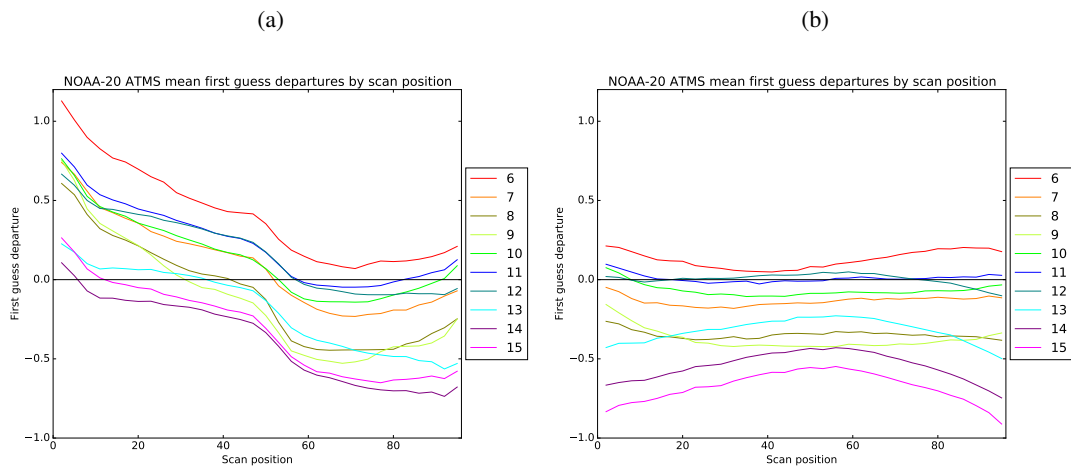
Figure 16: Mean first guess departures before bias correction binned by scan position for NOAA-20 ATMS temperature sounding channels 6 to 15 after (a) the original version of the antenna pattern correction and (b) the updated version of the antenna pattern correction. Statistics are for data after quality control and were accumulated between 22nd March 2018 and 12th April 2018

NOAA provided some test data with an updated antenna pattern correction which was assessed in the ECMWF assimilation system. Figure 16 (b) shows that the updated antenna pattern correction results in much more symmetric and smaller scan position dependent biases which VarBC is able to correct much more effectively. Comparing to figure 13 (a) shows that the biases for the data after antenna pattern correction are more symmetric and smaller in magnitude than the biases for the data before antenna pattern correction. The standard deviations of first guess departures are very slightly larger for the data after antenna pattern correction but in assimilation experiments there is neutral impact of switching from assimilating the data before antenna pattern correction to data after antenna pattern correction. Due to the smaller and more symmetric biases assimilating the SDRs is preferable to assimilating the TDRs.

With the corrected antenna pattern correction it is interesting to compare the biases for NOAA-20 ATMS

with Suomi-NPP ATMS and the temperature sounding channels of AMSU-A which, at time of writing, still has operational channels on six satellites. Figure 17 shows that the biases follow a similar pattern for most satellites with positive biases in the lowest peaking temperature sounding channel (ATMS channel 6 / AMSU-A channel 5). The biases become slightly more negative for the upper tropospheric temperature sounding channels (ATMS channels 7 to 9 / AMSU-A channels 6 to 8). The biases then become more positive for the lower stratospheric temperature sounding channels (ATMS channels 10 to 13 / AMSU-A channels 9 to 12). Finally the biases become more negative for the highest peaking stratospheric temperature sounding channels (ATMS channels 14 to 15 / AMSU-A channels 13 to 14). There is a spread of approximately 1K for each channel between the biases for the different satellites and instruments with the two ATMS instruments towards the lower end of this spread.

The grey markers and error bars in figure 17 are the estimated model bias and uncertainty. These are calculated by running a radiative transfer model on both GRUAN radiosonde and forecast model temperature and humidity profiles to produce the equivalent AMSU-A or ATMS channel brightness temperatures for the respective profiles. Then the difference between these produces an estimate of the model bias with respect to the GRUAN radiosonde measurements in brightness temperature space. The uncertainties are provided with the GRUAN radiosonde profiles and are also mapped into brightness temperature space. This was done as part of the GAIA-Clim project and Carminati et al. (2018, submitted) explains the methodology in more detail.
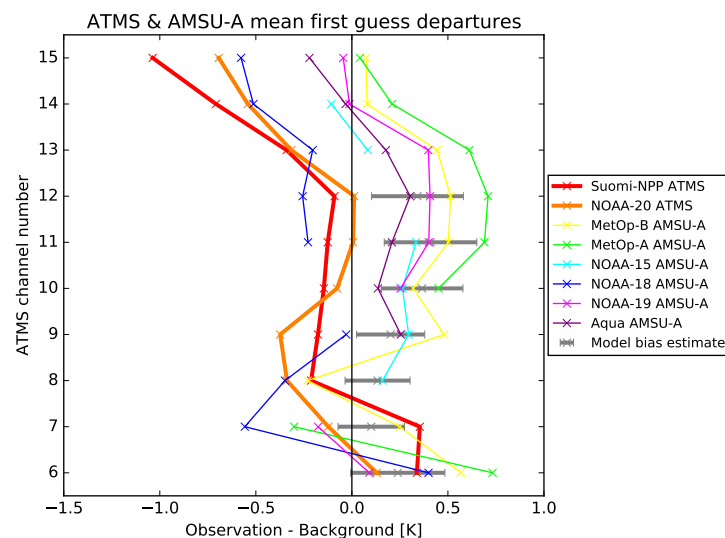
Figure 17: Global mean first guess departures for the ATMS temperature sounding channels onboard the NOAA-20 and Suomi-NPP satellites compared to the corresponding AMSU-A temperature sounding channels onboard the MetOp-A & B, NOAA-15, 18 & 19 and Aqua satellites (AMSU-A channel n corresponds to ATMS channel n+1). Statistics are for data after antenna pattern correction, after quality control, before bias correction has been applied and were accumulated between 1st and 10th April 2018. The grey markers and error bars represent the estimated model bias and uncertainty (see text for details)

Comparing the estimated model bias to the first guess departure biases in AMSU-A and ATMS suggests that most of the AMSU-A biases can be explained by model bias and that the bias coming from the observations is relatively small. For ATMS the first guess departure biases lie outside the model bias uncertainties which suggests that there is a significant contribution from observation biases for ATMS. This could partially be explained by a non-zero reflector emissivity for both Suomi-NPP and NOAA-20

ATMS which will be corrected for in 2019 (Tiger Yang, personal communication).

One enhancement of NOAA-20 over Suomi-NPP is that data from NOAA-20 ATMS arrives in a more timely manner with acquisition stations at McMurdo and Svalbard allowing for data to be downlinked twice per orbit as opposed to once per orbit for Suomi-NPP. This results in the average delay between the measurements being taken to the observations being ready for assimilation reducing from 100 minutes for Suomi-NPP to 50 minutes for NOAA-20. In the ECMWF early delivery suite (which is used to launch the operational forecasts which are delivered to member states) the observation cut off is 60 minutes. Currently, on average, 88% of Suomi-NPP ATMS data are available for assimilation in the early delivery cycles and this increases to 99% for NOAA-20 ATMS data. In the future with the move towards continuous data assimilation the impact of obtaining data with better timeliness will be even higher so this is a welcome enhancement for NOAA-20 over Suomi-NPP.

3.2 Experiments

Assimilation experiments were run to test the impact of assimilating the NOAA-20 ATMS data in addition to the full global observing system including Suomi-NPP ATMS. In the experiments summarised here the same configuration was used for NOAA-20 ATMS as is currently used for Suomi-NPP, again more details can be found in Bormann et al. (2013). In particular, the same inflated and diagonal observation errors are used despite the instrument noise being smaller for NOAA-20 ATMS than Suomi-NPP. Future work will focus on using more suitable correlated observation errors for NOAA-20 ATMS.

The same thinning is also used where one observation per 140km x 140km box and per 30 minute time slot is chosen. The 30 minute time slot is important for instruments onboard multiple satellites. NOAA-20 is in the same orbital plane as Suomi-NPP but they are half an orbit apart, so there is an approximate separation time of 50 minutes between NOAA-20 and Suomi-NPP passing over the same areas. This means that observations from the two satellites should never fall within the same timeslot and therefore observations from the two satellites are effectively thinned separately which should maximise the usage of ATMS on both satellites.

An experiment and control were run over one period of four months: 1st March 2018 to 30th June 2018. The experiment and control used the configuration of cycle 45r1 of the IFS and ran at $T_{CO}399$ (28km) forecast resolution with the first, second and third inner loops of the assimilation minimisation run at T_L95 (170km), T_L159 (120km) and T_L255 (80km) resolutions respectively. The control contained assimilation of the full observing system with the experiment additionally assimilating the NOAA-20 ATMS data before antenna pattern correction on top of this.

3.3 Results

Figure 18 shows that assimilating NOAA-20 ATMS improves the first guess fits to a number of independent observation types. Panel (a) shows improved first guess fits to most CrIS channels, particularly channels with wavenumbers between 661cm^{-1} and 704cm^{-1} which are sensitive to temperature in the stratosphere and upper troposphere. Also there are improved first guess fits to channels with wavenumbers around 1562cm^{-1} which are sensitive to upper tropospheric humidity. Panels (b) and (c) show improved first guess fits to all AMSU-A channels, particularly the stratospheric sensitive channels 9 to 14, and also to GPSRO bending angles, again particularly above 20km in the stratosphere. This indicates improved short-range forecasts of temperature, with the largest improvements in the stratosphere. Panels (d) and (e) show improved first guess fits to the humidity sensitive observations from the Geostationary

clear sky infrared radiances and MHS all sky microwave radiances. This indicates improved short-range forecasts of humidity and cloud. Finally, panel (f) shows improved first guess fits to conventional wind observations in the stratosphere indicating improved short-range forecasts of stratospheric wind.

Figure 19 shows that assimilating NOAA-20 ATMS leads to improvements to geopotential height forecasts in the stratosphere for lead times of 1 to 4 days. There are also smaller geopotential height increments and improvements to temperature and wind forecasts in the stratosphere (not shown). The impact in the troposphere is neutral at all lead times and also the impact in the stratosphere in the medium range is neutral.

This is the eighth microwave temperature sounding instrument to be assimilated in the ECMWF system and there is no sign that the impact has saturated yet. This may be because many of the AMSU-A instruments in orbit are ageing and a number of channels have malfunctioned and been blacklisted in recent years. The addition of NOAA-20 ATMS goes some way to replace those AMSU-A channels which can no longer be used and supplement the remaining AMSU-A and ATMS channels.
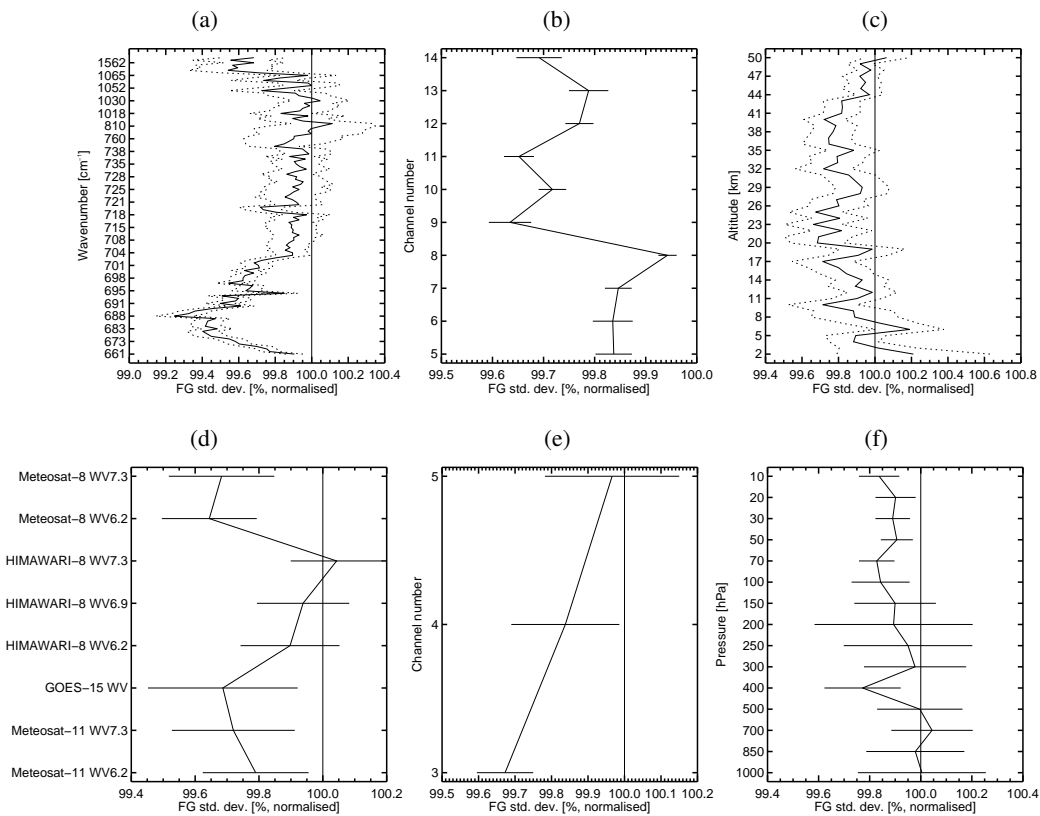
Figure 18: Change in standard deviation of first guess departures for (a) CrIS, (b) AMSU-A, (c) GPSRO, (d) Geostationary clear sky radiances, (e) MHS, and (f) conventional wind observations when adding the assimilation of NOAA-20 ATMS data against the control experiment

The largest impact of NOAA-20 ATMS appears to be in the stratosphere in both the change to first guess fits and the forecast scores. The model has some large temperature biases in the upper stratosphere (Shepherd et al., 2018) and the highest peaking microwave temperature sounding channels and GPSRO bending angles are the only observations capable of constraining the model globally at these levels. Recently an enhancement to VarBC called constrained VarBC (Han and Bormann, 2016) was introduced
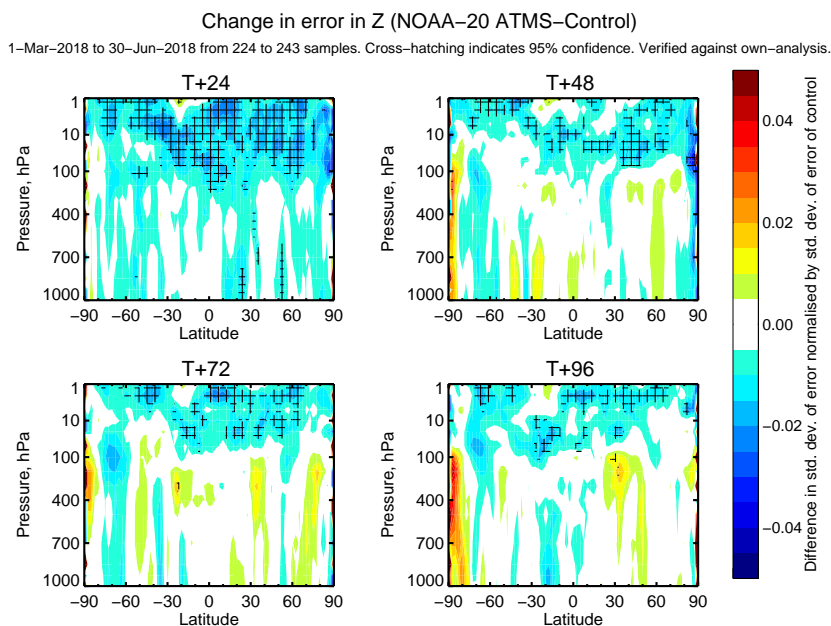
Figure 19: Change in standard deviation of geopotential height forecasts verified against own analyses when adding the assimilation of NOAA-20 ATMS against the control experiment

for these channels which allows for inter-satellite biases to be corrected and limits how much the applied bias correction is able to drift away from a correction of zero. This helps to control model biases at these levels and perhaps contributes to the positive impact in the stratosphere of NOAA-20 ATMS.

3.4 Summary

The data quality of NOAA-20 ATMS is generally comparable to or slightly better than Suomi-NPP ATMS. The biases are similar and VarBC is able to effectively correct both the scan and air mass dependent biases that are present in the first guess departure statistics. The instrument noise is lower for NOAA-20 ATMS than Suomi-NPP and this leads to significantly smaller standard deviations of first guess departures. It also appears that the contribution from the 1/f noise is reduced for NOAA-20 which means a much weaker striping signal is visible in the maps of first guess departures and also significantly weaker inter-channel error correlations. Over five months of monitoring the data quality appears to be stable.

Assimilation experiments show that assimilating the NOAA-20 ATMS data on top of the full observing system results in small but significant improvements to short-range forecasts of temperature, humidity and wind, particularly in the stratosphere, as measured by improved first guess fits to independent observations sensitive to these variables. In addition assimilating NOAA-20 ATMS data results in smaller geopotential height increments and improved short-range geopotential height forecasts in the stratosphere. Medium range forecast impact is neutral.

These results led to the decision to start assimilating NOAA-20 ATMS TDRs in operations from 22nd May 2018.

In June 2018 an updated antenna pattern correction was applied to the NOAA-20 ATMS data which resulted in much better quality SDRs with smaller and more symmetric biases than the TDRs. After a short assessment period the operational assimilation of NOAA-20 ATMS was switched from the TDRs

to the SDRs on 1st August 2018.

4   Future work

From cycle 46r1 the treatment of assigned observation errors will be inconsistent between Suomi-NPP ATMS, which will use a correlated observation errors, and NOAA-20 ATMS, which will use the inflated, diagonal observation errors. To address this, work is underway to account for correlated errors for NOAA-20 ATMS too. Experiments using correlated errors for NOAA-20 ATMS produced using the same methods as for Suomi-NPP ATMS (x1.75 inflation of Desroziers diagnosed error covariance matrix) have shown that the degradations to the tropopause sensitive channels have worsened, see the red line of figure 20 around wavenumber 695cm^{-1}. However, using matrices where the smallest eigenvalues have been inflated improve the first guess fits to these tropopause sensitive channels, see the black line of figure 20 around wavenumber 695cm^{-1}. A more thorough impact assessment of these experiments will be necessary before this can be implemented in operations but the initial results are promising which will hopefully lead to a consistent treatment of correlated errors for both Suomi-NPP and NOAA-20 ATMS.
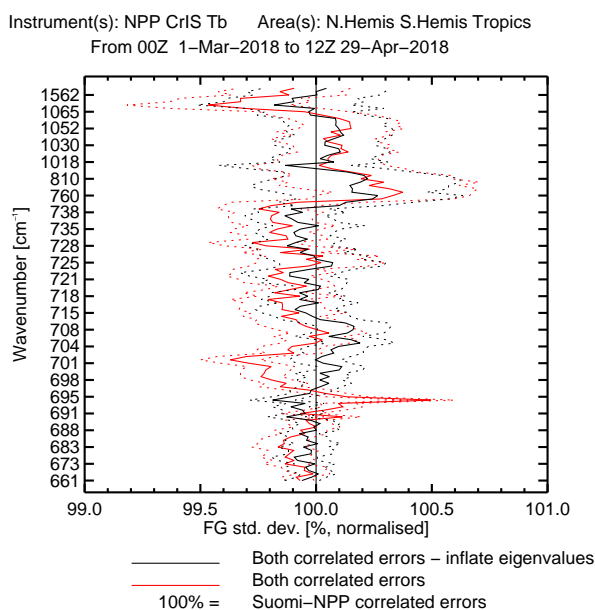
Figure 20: Change in global standard deviation of first guess departures for CrIS when ATMS correlated errors are used just for Suomi-NPP ATMS (100% line), for both Suomi-NPP and NOAA-20 ATMS (red line) and for both Suomi-NPP and NOAA-20 ATMS but with the smallest eigenvalues inflated (black line)

Once a consistent set of observation errors are being used for both Suomi-NPP and NOAA-20 ATMS it would be interesting to assess the forecast sensitivity to observation impact (FSOI). The results for NOAA-20 ATMS could be compared to Suomi-NPP ATMS and the AMSU-A instruments on different satellites to see whether the lower noise leads to increased impact by that metric. It would also be interesting to see the change in FSOI when correlated errors for Suomi-NPP ATMS is introduced.

In November 2018 the launch of the third EUMETSAT MetOp satellite, MetOp-C, is expected. This satellite will carry onboard the final AMSU-A and MHS instruments. As with NOAA-20 ATMS, once MetOp-C is launched the data quality of the AMSU-A and MHS instruments will be assessed and, if

good, assimilation experiments will be run to assess the impact of assimilating these instruments on top of the current system. It will be interesting to see whether the impact of new microwave sounder data has saturated or whether the assimilation of these two instruments leads to further improvements.

Finally, work is still underway on moving the assimilation of AMSU-A from the clear sky system to the all sky system and this will be the subject of a future report.

Acknowledgements

References

Anderson, E., Järvinen, H., 1999. Variational quality control. Quarterly Journal of the Royal Meteorological Society 125 (554), 697–722.
URL https://rmets.onlinelibrary.wiley.com/doi/abs/10.1002/qj.49712555416

Bormann, N., Bauer, P., 2010. Estimates of spatial and interchannel observation-error characteristics for current sounder radiances for numerical weather prediction. I: Methods and application to ATOVS data. Q.J.R.Meteorol.Soc. 136, 1036–1050.

Bormann, N., Bonavita, M., Dragani, R., Eresmaa, R., Matricardi, M., McNally, A., 2016. Enhancing the impact of IASI observations through an updated observationerror covariance matrix. Quarterly Journal of the Royal Meteorological Society 142 (697), 1767–1780.
URL https://rmets.onlinelibrary.wiley.com/doi/abs/10.1002/qj.2774

Bormann, N., Collard, A., Bauer, P., 2011. Observation errors and their correlations for satellite radiances. ECMWF Newsletter 128, 17–22.

Bormann, N., Fouilloux, A., Bell, W., 2013. Evaluation and assimilation of ATMS data in the ECMWF system. Journal of Geophysical Research: Atmospheres 118 (23), 12,970–12,980.
URL https://agupubs.onlinelibrary.wiley.com/doi/abs/10.1002/2013JD020325

Campbell, W. F., Satterfield, E. A., Ruston, B., Baker, N. L., 2017. Accounting for correlated observation error in a dual-formulation 4D variational data assimilation system. Monthly Weather Review 145 (3), 1019–1032.
URL https://doi.org/10.1175/MWR-D-16-0240.1

Carminati, F., Migliorini, S., Ingleby, B., Bell, W., Lawrence, H., Newman, S., Hocking, J., Smith, A., 2018, submitted. Using reference radiosondes to characterise NWP model uncertainty for improved satellite calibration and validation. Atmos. Meas. Tech.

Desroziers, G., Berre, L., Chapnik, B., Poli, P., 2005. Diagnosis of observation, background and analysis-error statistics in observation space. Quarterly Journal of the Royal Meteorological Society 131 (613), 3385–3396.
URL https://rmets.onlinelibrary.wiley.com/doi/abs/10.1256/qj.05.108

Eyre, J. R., Hilton, F. I., 2013. Sensitivity of analysis error covariance to the mis-specification of background error covariance. Quarterly Journal of the Royal Meteorological Society 139 (671), 524–533.
URL https://rmets.onlinelibrary.wiley.com/doi/abs/10.1002/qj.1979

Geer, A., Baordo, F., Bormann, N., English, S., 2014. All-sky assimilation of microwave humidity sounders. Technical Memorandum 741.

Geer, A. J., 2016. Significance of changes in medium-range forecast scores. Tellus A: Dynamic Meteorology and Oceanography 68 (1), 30229.
URL https://doi.org/10.3402/tellusa.v68.30229

Han, W., Bormann, N., 2016. Constrained adaptive bias correction for satellite radiance assimilation in the ECMWF 4D-Var system. Technical Memorandum 783.

Hollingsworth, A., Lönnberg, P., 1986. The statistical structure of shortrange forecast errors as determined from radiosonde data. Part I: The wind field. Tellus A 38A (2), 111–136.
URL https://onlinelibrary.wiley.com/doi/abs/10.1111/j.1600-0870.1986.tb00460.x

Kim, E., Lyu, C.-H. J., Anderson, K., Leslie, R. V., Blackwell, W. J., 2014. S-NPP ATMS instrument prelaunch and on-orbit performance evaluation. Journal of Geophysical Research: Atmospheres 119 (9), 5653–5670.
URL https://agupubs.onlinelibrary.wiley.com/doi/abs/10.1002/2013JD020483

Lawrence, H., Bormann, N., 2014. First year report: The impact of HIRS on ECMWF forecasts, adding ATMS data over land and sea ice and new observation errors for AMSU-A. EUMETSAT/ECMWF Fellowship Programme Research Report No.34.

Lawrence, H., Bormann, N., English, S., 2015. Scene-dependent observation errors for the assimilation of AMSU-A. EUMETSAT/ECMWF Fellowship Programme Research Report No.39.

Lonitz, K., Geer, A. J., 2017. Effect of assimilating microwave imager observations in the presence of a model bias in marine stratocumuls. EUMETSAT/ECMWF Fellowship Programme Research Report No.44.

Shepherd, T., Polichtchouk, I., Hogan, R., Simmons, A., 2018. Report on stratosphere task force. Technical Memorandum 824.

Weston, P., Bormann, N., Geer, A., Lawrence, H., 2017. Harmonisation of the usage of microwave sounder data over land, coasts, sea ice and snow: First year report. EUMETSAT/ECMWF Fellowship Programme Research Report No.45.

Weston, P. P., Bell, W., Eyre, J. R., 2014. Accounting for correlated error in the assimilation of highresolution sounder data. Quarterly Journal of the Royal Meteorological Society 140 (685), 2420–2429. URL https://rmets.onlinelibrary.wiley.com/doi/abs/10.1002/qj.2306